THE JOURNAL OF BIOLOGICAL CHEMISTRY VOL. 287, NO. 4, pp. 2863–2876, January 20, 2012

Gene Dose Influences Cellular and Calcium Channel Dysregulation in Heterozygous and Homozygous T4826I-RYR1 Malignant Hyperthermia-susceptible Muscle*[S]

Received for publication, September 26, 2011, and in revised form, November 16, 2011 Published, JBC Papers in Press, December 2, 2011, DOI 10.1074/jbc.M111.307926

Genaro C. Barrientos[‡1], Wei Feng[‡1], Kim Truong[‡], Klaus I. Matthaei[§], Tianzhong Yang[¶], Paul D. Allen[¶], José R. Lopez[¶], and Isaac N. Pessah[‡2]

From the [‡]Department of Molecular Biosciences, School of Veterinary Medicine, University of California, Davis, California 95616, the [§]John Curtin School of Medical Research, Australian National University, Canberra, ACT 0200, Australia, and the [¶]Department of Anesthesiology, Brigham and Women's Hospital, Boston, Massachusetts 02115

Background: Muscle from heterozygous and homozygous T4826I-RYR1 MH-susceptible mice is investigated for biochemical and cellular abnormalities.
Results: T4826I-RYR1 gene dose determines severity of $[Ca^{2+}]_{rest}$, mitochondrial, EC coupling, and Ca^{2+} channel impairments.
Conclusion: T4826I-RYR1 channel dysfunction is regulated *in vivo* but imparts susceptibility to environmental triggers.
Significance: T4826I-RYR1 is sufficient to confer MHS strongly dependent on gene dose.

Malignant hyperthermia susceptibility (MHS) is primarily conferred by mutations within ryanodine receptor type 1 (RYR1). Here we address how the MHS mutation T4826I within the S4-S5 linker influences excitation-contraction coupling and resting myoplasmic Ca^{2+} concentration ($[Ca^{2+}]_{rest}$) in flexor digitorum brevis (FDB) and vastus lateralis prepared from heterozygous (Het) and homozygous (Hom) T4826I-RYR1 knock-in mice (Yuen, B. T., Boncompagni, S., Feng, W., Yang, T., Lopez, J. R., Matthaei, K. I., Goth, S. R., Protasi, F., Franzini-Armstrong, C., Allen, P. D., and Pessah, I. N. (2011) *FASEB J.* doi:22131268). FDB responses to electrical stimuli and acute halothane (0.1%, v/v) exposure showed a rank order of Hom ≫ Het ≫ WT. Release of Ca^{2+} from the sarcoplasmic reticulum and Ca^{2+} entry contributed to halothane-triggered increases in $[Ca^{2+}]_{rest}$ in Hom FDBs and elicited pronounced Ca^{2+} oscillations in ~30% of FDBs tested. Genotype contributed significantly elevated $[Ca^{2+}]_{rest}$ (Hom > Het > WT) measured *in vivo* using ion-selective microelectrodes. Het and Hom oxygen consumption rates measured in intact myotubes using the Seahorse Bioscience (Billerica, MA) flux analyzer and mitochondrial content measured with MitoTracker were lower than WT, whereas total cellular calpain activity was higher than WT. Muscle membranes did not differ in RYR1 expression nor in Ser^{2844} phosphorylation among the genotypes. Single channel analysis showed highly divergent gating behavior with Hom and WT favoring open and closed states, respectively, whereas Het exhibited heterogeneous gating behaviors. [^{3}H]Ryanodine binding analysis revealed a gene dose influence on binding density and regulation by Ca^{2+}, Mg^{2+}, and temperature. Pronounced abnormalities inherent in T4826I-RYR1 channels confer MHS and promote basal disturbances of excitation-contraction coupling, $[Ca^{2+}]_{rest}$, and oxygen consumption rates. Considering that both Het and Hom T4826I-RYR1 mice are viable, the remarkable isolated single channel dysfunction mediated through this mutation in S4-S5 cytoplasmic linker must be highly regulated *in vivo*.

Fulminant malignant hyperthermia (MH)[3] is a pharmacogenetic, life-threatening syndrome triggered in susceptible individuals by volatile general anesthetics, depolarizing neuromuscular blocking agents, and heat stress (2). An MH episode is characterized by increased expired CO_2, rapid onset of metabolic acidosis, elevated core temperature, and sustained muscle contraction. Such episodes are often associated with ventricular tachycardia and cardiac arrest. The prevalence of MH has been estimated as 1 in 10,000 anesthetic procedures; however, this is likely to be an underestimate of MH susceptibility in the general population, which has been estimated as high as 1:2,000 (3–5).

Although seven genomic loci have been linked to the disorder (6, 7), mutations in only two skeletal muscle proteins have been confirmed to confer MH susceptibility. At least 250 mutations within the *RYR1* locus (19q13.1) that encodes for the type 1 ryanodine receptor (RYR1), a Ca^{2+} channel that localizes within skeletal muscle junctional sarcoplasmic reticulum (SR), have been associated with human MH susceptibility (4, 8–10). RYR1 mutations currently account for more than 50% of the families identified (4). More recently, a small number of mutations in *CACNA1S* (1q32) that encode for the pore-forming

* This work was supported, in whole or in part, by National Institutes of Health Grants 1P01 AR52354 and 3R01 AR043140 (to P. D. A. and I. N. P.) and 1R01 ES014901 (to I. N. P.). This work was also supported by a grant from the J. B. Johnson Foundation.
[S] This article contains supplemental Movie 1.
[1] Both authors contributed equally to this work.
[2] To whom correspondence should be addressed: Molecular Biosciences, University of California Davis, One Shields Ave., Davis, CA 95616. Tel.: 530-752-6696; Fax: 530-752-4698; E-mail: inpessah@ucdavis.edu.

[3] The abbreviations used are: MH, malignant hyperthermia; MHS, MH susceptibility; SR, sarcoplasmic reticulum; EC, excitation-contraction; Het, heterozygous; Hom, homozygous; OCR, oxygen consumption rate; FCCP, carbonyl cyanide *p*-trifluoromethoxyphenylhydrazone; *t*-Boc, *tert*-Boc-L-leucyl-L-methionine amide; Ry, ryanodine; $[Ca^{2+}]_{rest}$, resting Ca^{2+} concentration; RC, respiratory capacity; PP1, protein phosphatase 1; DHPR, dihydropyridine receptor; MHS, BLM, bilayer lipid membrane.

subunit ($Ca_V1.1$; α_{1s}DHPR) of the L-type voltage-dependent Ca^{2+} channels that localize within the skeletal muscle T-tubule membrane were also confirmed to confer MH susceptibility. Confirmed cases include three families with R1086H (11, 12), one family with R1086S (13), and another with the R174W mutation (14). One theory currently being tested is that MH mutations in either $Ca_V1.1$ or RYR1 alter the fidelity of bidirectional signaling across T-tubule SR junctions that is essential for normal skeletal muscle excitation-contraction (EC) coupling (15) and regulation of SR Ca^{2+} leak (16).

Knock-in mice heterozygous (Het) for missense mutation R163C-RYR1 (17) or Y522S-RYR1 (18), two of the more common mutations conferring MH susceptibility in humans, exhibit fulminant MH when exposed to either an inhaled volatile general anesthetic (*e.g.* halothane) or heat stress. Homozygous (Hom) R163C-RYR1 and Y522S-RYR1 mice are not viable, whereas their Het counterparts maintain MH susceptibility throughout a normal life span. Both mouse models have contributed valuable information about how N-terminal mutations affect basal RYR1 channel dysfunction and alter pharmacological responses of intact muscle cells (19, 20). Y522S-RYR1 mice show temporal development of skeletal muscle lesions resembling central core disease in humans (21), whereas Het R163C-RYR1 mice appear to have minimal muscle pathology.[4] These observations in mice are not consistent with clinical evidence indicating that both analogous mutations cause MH susceptibility in humans and that both are associated with central core disease, although the onset and patterns of muscle damage can differ (7, 22). Importantly muscle cells expressing either RYR1 mutation led to three fundamentally important findings about MH susceptibility: 1) both show evidence of altered patterns of bidirectional signaling between $Ca_V1.1$ and RYR1, with activation of L-type Ca^{2+} current shifted to more negative potentials (23–25); 2) both have chronically elevated cytoplasmic resting Ca^{2+} measured both *in vitro* (26) and *in vivo* (19, 27); and 3) both have basal alterations in mitochondrial functions that increase production of reactive oxygen species (20, 28). Why Y522S-RYR1 and R163C promote different patterns of skeletal muscle damage is not understood.

Recently, we completed phenotyping a new MHS mouse expressing a mutation within the C-terminal region of RYR1, T4826I-RYR1 (1), a mutation first described in a New Zealand Maori pedigree with MH susceptibility but no clinical evidence of central core disease (29). T4826I-RYR1 mice have several notable phenotypic differences compared with mice expressing N-terminal mutations. Both Het and Hom T4826I-RYR1 mice survive to maturity and show marked genotype and gender differences in susceptibility to triggered MH with halothane and/or heat stress throughout their life span. Electron micrographic assessment of soleus indicates late onset alterations, including abnormally distributed and enlarged mitochondria, deeply infolded sarcolemma, and frequent z-line streaming regions, which are more severe in males (1). Collectively, these data indicate that the location of a mutation within the RYR1 sequence influences not only the penetrance and gender dependence of MH susceptibility but also the patterns of basal changes in muscle bioenergetics and the progression and extent of muscle damage.

Here we report a detailed analysis of basal functional differences in EC coupling and resting cytoplasmic Ca^{2+} that confer heightened sensitivity to halothane in single FDB fibers prepared from Het and Hom T4826I-RYR1 knock-in mice and how these differences relate to inherent biochemical and biophysical alterations in RYR1 Ca^{2+} channels. We also find that intact myotubes derived from either Het or Hom T4826I-RYR1 have altered oxygen consumption rates when compared with WT.

EXPERIMENTAL PROCEDURES

Animals—WT, Het, and Hom skeletal muscle tissue, FDB fibers, and myotubes were obtained from Het × Het crosses of the T4826I-RYR1 knock-in mouse line (back-bred at least 10 generations to the C57BL/6 line) as described previously (1). All cellular and biochemical experiments were performed from tissues collected from mice whose genotype was determined by PCR screening. The PCR primer sequences were as follows: T4826I-RYR1 (forward), TTT GGA GAC ACG GAA ACA GAA; T4826I-RYR1 (reverse), AGG GAG GTA CCT GGC ACT CA; WT-RYR1 (forward), TCT CAC TGT CCA TAG CTG; WT-RYR1 (reverse), ATC CAG CTT CTC CTA CAG. All experiments on animals and collections of animal tissues for the studies were conducted using protocols approved by the institutional animal care and use committees at the University of California at Davis.

Preparation of Primary Myotubes and Adult FDB Fibers—Primary skeletal myoblast lines were isolated from newborn WT mice or mice verified Het or Hom for T4826I-RYR1 as described previously (30–32). The myoblasts were expanded in 10-cm cell culture-treated Corning dishes coated with collagen (Calbiochem) and were plated onto 96-well μ-clear plates (Greiner) coated with Matrigel (BD Biosciences) for detection of calpain or mitochondrial content or were alternatively seeded onto proprietary 12-well plates for measuring oxygen consumption (Seahorse Biosciences). Upon reaching ~80% confluence, growth factors were withdrawn, and the cells were allowed to differentiate into myotubes over a period of 3 days for these analyses (see below).

Flexor digitorum brevis (FDB) muscles were dissected from male 3–6-month-old mice verified by PCR as WT, Het or Hom T4826I-RYR1 genotype. Single intact myofibers were enzymatically isolated as described previously (19, 33). In order to reduce stress-activated SR Ca^{2+} release during isolation, especially in T4826I-RYR1 fibers, 10 μM dantrolene was included in the initial dissociation medium. After isolation, the fibers were plated on Matrigel-coated plates (BD Biosciences) and maintained in Dulbecco's modified Eagle's medium (Invitrogen) supplemented with 10% fetal bovine serum (Thermo Fisher Scientific, Waltham, MA) and 0.1 mg/ml penicillin-streptomycin (Sigma) in the absence of dantrolene. Fibers were kept overnight in a 5% CO_2 incubator, and experiments were conducted within 12–24 h of plating.

Ca^{2+} Imaging—FDB fibers were loaded with Fluo-4/AM (10 μM; 40 min at room temperature) in normal Ringer solution

[4] C. Franzini-Armstrong, personal communication.

containing 146 mM NaCl, 4.7 mM KCl, 0.6 mM $MgSO_4$, 6 mM glucose, 25 mM HEPES, 2 mM $CaCl_2$, and 0.02% Pluronic® F-127 (Invitrogen). The cells were then washed three times with Ringer's solution and transferred to the stage of an IX71 inverted microscope equipped with a 40 × 0.9 numerical aperture objective (Olympus, Center Valley, PA) and illuminated at 494 nm to excite Fluo-4 with a DeltaRam wavelength-selectable light source. Fluorescence emission at 510 nm was captured from individual fibers. Electrical field stimuli were applied using two platinum electrodes fixed to opposite sides of the well and connected to an A.M.P.I. Master 8 stimulator set at 4 V, 0.5-ms bipolar pulse duration over a range of frequencies (1–20 Hz; 10-s pulse train duration). Fluo-4 fluorescence emission was measured at 30 frames/s using a Cascade Evolve 512 camera (Photometrics, Tucson, AZ). The images were acquired using the Easy Ratio Pro software (PTI). The data were analyzed using Origin 7 software (OriginLab Corp.). Transients were normalized to the florescence base line (F_o) of each individual fiber, and the integrated area within the evoked responses was calculated from the number of fibers indicated in the figure legend. Statistical comparisons were performed with an unpaired *t* test.

In Vivo Recording of V_m and $[Ca^{2+}]_{rest}$—Measurements were performed on mice sedated with non-triggering ketamine/xylazine (100/5 mg/kg), and core temperature was maintained euthermic with an automated heating system (ATC1000 WPI). Once anesthesia was confirmed by a loss of tail pinch response, mice were intubated with a tracheal cannula and connected to a ventilator (Harvard Minivent, M-845, Holliston, MA) set at a stroke volume of 200 μl, 180 stokes/min, and ventilated with medical air. Small incisions were made to expose the vastus lateralis muscle of the left leg, and muscle fibers were impaled with the double-barreled microelectrode as described previously (19). Potentials were recorded via a high impedance amplifier (WPI FD-223, Sarasota, FL). The potential from the 3 M KCl barrel (V_m) was subtracted electronically from V_{CaE}, to produce a differential Ca^{2+}-specific potential (V_{Ca}) that represents the $[Ca^{2+}]_{rest}$. V_m and V_{Ca} were filtered (30–50 kHz) to improve the signal/noise ratio and stored in a computer for further analysis.

Halothane Exposure—Dissociated fibers were perfused with 0.1% (v/v) halothane freshly prepared in the imaging solution. The halothane concentration was confirmed by mass spectrometry (23).

Seahorse XF-24 Metabolic Flux Analysis—Myoblasts were cultured on Matrigel-coated Seahorse XF-24 plates (Seahorse Biosciences) at a density of 30,000 cells/well using the same procedure described above for Ca^{2+} imaging experiments. The oxygen consumption rate (OCR) and extracellular acidification rate were evaluated after 3 days of differentiation. Before the experiment, the myotubes were equilibrated in DMEM supplemented with 1 mM pyruvate and 1 mM GlutaMAX (running medium) during 1 h at 37 °C. The oligomycin (10 μg/ml final concentration), FCCP (1 μM final concentration), and rotenone (0.1 μM final concentration) were dissolved in the running medium. The respiratory capacity is defined like the OCR after the FCCP addition. To compare the respiratory capacity among the three genotypes, we calculated the area under the curve. Values were normalized using the protein content of each well.

Mitochondria Content—Mitochondria content was quantified by staining myotubes with MitoTracker Green (Invitrogen), which preferentially accumulates in mitochondria regardless of the of the mitochondrial membrane potential and provides an accurate assessment of total mitochondrial mass (34, 35). Briefly, myotubes were loaded with 100 nM MitoTracker Green for 30 min at 37 °C. The myotubes were trypsinized and washed by centrifugation, and the associated fluorescence was measured (excitation/emission 516/490 nm). The fluorescence values were normalized using the protein concentration.

Calpain Activity—The peptidase activity was evaluated using the synthetic substrate *tert*-Boc-L-leucyl-L-methionine amide (*t*-Boc) (Invitrogen) (36). Skeletal myotubes were loaded with 10 μM *t*-Boc for 30 min at 37 °C. After cleavage by peptidases, the product produces blue fluorescence with excitation and emission maxima of ~351 and 430 nm, respectively. In order to compare the fluorescence among the different genotypes, we performed the assay using the Quantum View feature of an Evolve 512 digital camera, permitting electron counting of each pixel in the image. Measurements were captured from regions of interest of identical size for each myotube, and the intensity values were averaged for each genotype under identical illumination conditions on the same day.

Preparations of Membrane Fractions from Mouse Skeletal Muscle—Skeletal muscles collected from male WT-RYR1, Het, or Hom T4826I-RYR1 mice (2–3 animals/preparation, 3–6 months of age) were either prepared from freshly isolated tissue or tissue flash-frozen and stored in liquid nitrogen and stored at −80 °C. Fresh tissue was minced on ice (frozen tissue was pulverized) and placed in ice-cold buffer containing 300 mM sucrose, 5 mM imidazole, 0.1 mM PMSF, and 10 μg/ml leupeptin, pH 7.4, and homogenized with three sequential bursts (30 s each) of a PowerGen 700D (Fisher), at 9,000, 18,000, and 18,000 rpm. Homogenates were centrifuged at 10,000 × *g* for 20 min. Supernatants were saved, whereas the pellets were subjected to a second round of homogenization and centrifugation at the same settings described above. The remaining pellets were discarded, and the supernatants were combined and poured through four layers of cheesecloth. The filtrate was centrifuged at 110,000 × *g* for 60 min at 4 °C. Pellets were resuspended in 300 mM sucrose, 10 mM Hepes, pH 7.4, aliquoted into microcentrifuge tubes (100 μl/sample), and either stored at −80 °C for biochemical analyses or subjected to further purification to obtain membranes enriched in junctional SR as described previously by Saito *et al.* (37). Protein concentration for each preparation was determined using the DC protein assay kit (Bio-Rad).

Measurements of [^{3}H]Ryanodine Binding—The apparent association or equilibrium binding of [^{3}H]ryanodine ([^{3}H]Ry) to RYR1-enriched membrane preparation (0.1–0.15 mg/ml) was measured at 25 or 37 °C for 0–3 h with constant shaking in buffer consisting of 2–5 nM [^{3}H]Ry (PerkinElmer Life Sciences), 250 mM KCl, 20 mM HEPES, pH 7.4 (38), and defined free $[Ca^{2+}]$ as indicated in each specific experiment. Free Ca^{2+} was obtained by the addition of EGTA calculated according to the software Bound-and-Determined (39). RYR1 channel modulators Ca^{2+} and/or Mg^{2+} were titrated in specific experiments as

described in the figure legends. Nonspecific [^{3}H]Ry binding was determined in the presence of a 1,000-fold excess of unlabeled ryanodine. Bound and free ligand were separated by rapid filtration through Whatman GF/B glass fiber filters using a Brandel cell harvester (Whatman, Gaithersburg, MD) with three washes with 5 ml of ice-cold buffer (250 mM KCl, 20 mM HEPES, 15 mM NaCl, and 50 μM Ca^{2+}, pH 7.4). [^{3}H]Ry retained in filters was quantified by liquid scintillation spectrometry using a scintillation counter (Beckman model 6500). Each experiment was performed on at least two independent skeletal muscle preparations, each in triplicate. Linear or non-linear curve fitting was performed using Origin® software (Northampton, MA).

Measurements and Analyses of Single RYR1 Channels in Bilayer Lipid Membrane (BLM)—Skeletal muscle membrane preparation was used in order to induce fusion with the planar BLM. BLM was formed by 30 mg/ml phosphatidylethanolamine/phosphatidylserine/phosphatidylcholine in decane (5:3:2 (w/w/w); Avanti Polar Lipids, Inc., Alabaster, AL). A 10-fold Cs^+ gradient was built from *cis* to *trans* (500 to 50 mM). The recording baths were buffered to pH 7.4 by 20 mM Hepes. The holding potential was held at −40 mV by bilayer clamp BC 525C (Warner Instruments, Hampden, CT) on the *trans* side, where *cis* was virtually grounded. The *cis* chamber was where membrane protein was added and thus was actually the cytosolic face of the incorporated channel. The acquired current signals, filtered at 1 kHz (low pass Bessel Filter 8 Pole; Warner Instruments) were digitized and acquired at a sampling rate of 10 kHz (Digidata 1320A, Molecular Devices (Sunnyvale, CA)). All current recordings were made with Axoscope 10 software (Molecular Devices) for at least 1 min under each defined experimental condition. The channel open probability (P_o), mean open and closed dwell times (τ_o and τ_c), and current histograms were calculated and obtained using Clampfit, pClamp software version 10.0 (Molecular Devices). The number of channels recorded under each condition was specified in the respective figure legends. Differences in the WT-RYR1, Het, and Hom T4826I-RYR1 P_o values were tested for statistical significance using unpaired Student's *t* tests.

Western Blotting—Skeletal muscle (genders either pooled or separated by genotype) was homogenized, and crude membrane fractions were prepared and denatured in SDS-PAGE sample buffer (Bio-Rad) containing 5% 2-mercaptoethanol at 80 °C for 5 min. Protein (5, 10, or 15 μg/lane) was loaded onto Tris acetate 4–12% or 7% acrylamide gradient SDS-polyacrylamide gels (Invitrogen), electrophoresed, blotted onto PVDF, labeled using secondary antibodies conjugated to infrared dyes (emission 700 or 800 nm), and imaged using a LI-COR imager as described previously (19). Total RYR1 was detected with antibody 34C (40) at 1:1,000 dilution (Developmental Studies Hybridoma Bank, University of Iowa, Iowa City). Phosphoepitope-specific antibody that recognizes mouse RYR1 Ser^{2844}, a PKA phosphorylation site (41), was purchased from Abcam (ab59225) and used at 1:2,000 dilution. Band intensities of RYR1 were normalized to glyceraldehyde 3-phosphate dehydrogenase (GAPDH) as a measure of total RYR1 protein, and intensity of the Ser(P)^{2844}-RYR1/total RYR1 ratio was analyzed using Odyssey version 3.0 software. Protein phosphatase 1 (PP1; New England Biolabs) was utilized to dephosphorylate SR protein according to the vendor's instructions. The reaction mixture contained 50 mM HEPES, 100 mM NaCl, 2 mM DTT, 1 mM $MnCl_2$, 0.01% Brij 35, pH 7.5, 4 mg/ml membrane protein (WT, Het, and Hom T4826I-RYR1), and 200 units/ml PP1, which was incubated at 30 °C for 10 min. Then the samples were diluted into SDS-PAGE sample buffer for Western blotting or into [^{3}H]Ry binding buffer. [^{3}H]Ry binding assay was performed with 5 nM [^{3}H]Ry, 1 μM free Ca^{2+}, 100 μg/ml proteins in binding buffer containing 250 mM KCl and 20 mM Hepes, pH 7.4, at 37 °C for 3 h.

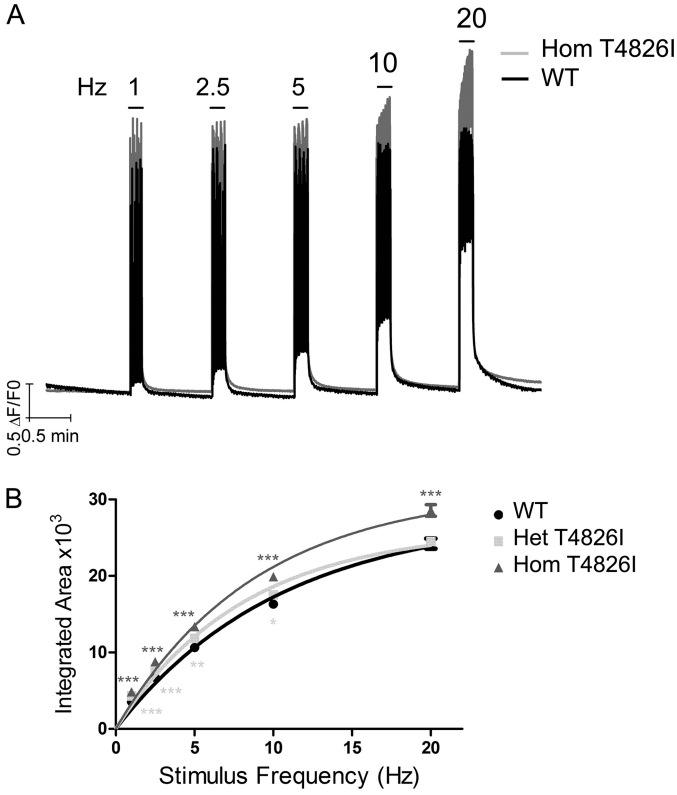

FIGURE 1. **T4826I knock-in fibers display an enhanced frequency response compared with the WT fibers.** Fibers dissociated from WT-RYR1, Het T4826I-RYR1, or Hom T4826I-RYR1 mice were loaded with Fluo-4 and tested for electrically evoked EC coupling in the Ca^{2+}-replete external buffer ($[Ca^{2+}]_e$ = 2 mM). *A*, representative responses of FDB to electrical pulse trains applied at 1–20 Hz for a 10-s duration isolated from WT (*black trace*) and Hom T4826I-RYR1 (*gray trace*) mice. For clarity, the Het T4826I-RYR1 trace is not superimposed on the traces. *B*, summary data for all three genotypes relating integrated areas of the Ca^{2+} transient at each stimulus frequency. WT-RYR1 results are mean data ± S.E. from n = 162 fibers from five animals; Het results are from n = 180 fibers from three animals, and Hom results are from n = 203 fibers from four animals. ***, $p < 0.001$ compared with WT. **, $p < 0.01$ compared with WT. *, $p < 0.05$ compared with WT.

RESULTS

T4826I-RYR1 FDB Fibers Display Enhanced Ca^{2+} Transient Properties and Heightened Sensitivity to Halothane—Differences in EC coupling in FDB fibers isolated from male WT mice and knock-in Het or Hom T4826I-RYR1 were measured by imaging electrically evoked Ca^{2+} transients with Fluo-4. FDB fibers were sequentially stimulated at frequencies ranging from 1 to 20 Hz, and the magnitude of the Ca^{2+} transients was quantified as the integrated area of the response. Fig. 1*A* shows representative traces of electrically evoked Ca^{2+} transients measured in WT and Hom T4826I-RYR1 myotubes superimposed.

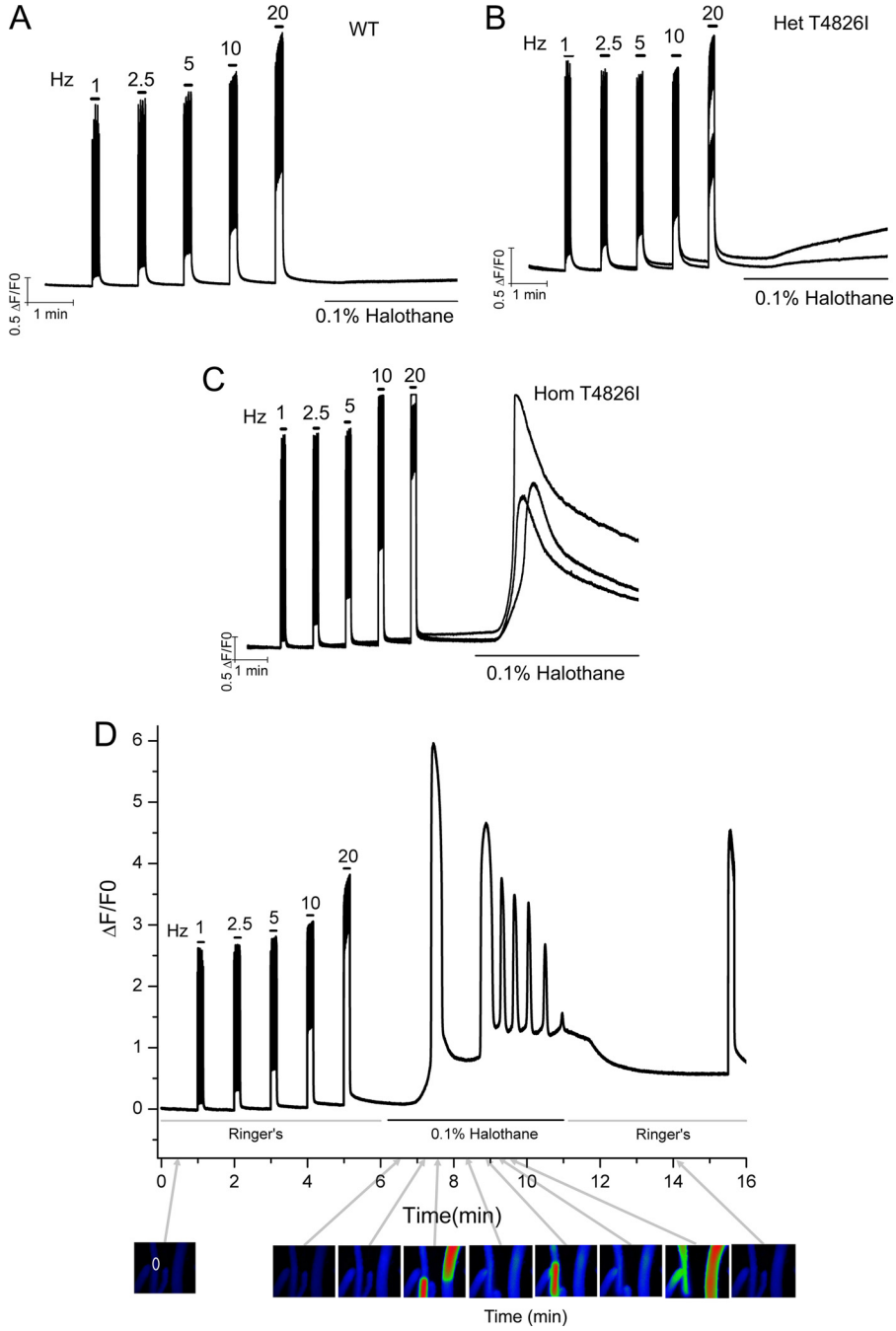

FIGURE 2. **Het and Hom T4826I-RYR1 FDB fibers show heightened sensitivity to halothane.** Fibers dissociated from WT-RYR1 (*A*), Het T4826I-RYR1 (*B*), or Hom T4826I-RYR1 (*C*) mice were loaded with Fluo-4 and tested for electrically evoked EC coupling in the Ca^{2+} replete external buffer ($[Ca^{2+}]_e = 2$ mM). Fibers were then challenged with halothane dissolved in the same external buffer ($[Ca^{2+}]_e = 2$ mM) in the absence of electrical stimuli. *A–C*, traces from individual fibers from each genotype. Similar results were obtained from 39 and 28 Het and Hom fibers, respectively, from three independent fiber isolations for each genotype. *D*, halothane can produce marked elevation in base-line Ca^{2+} and regenerative Ca^{2+} waves that were observed in eight of 28 Hom T4826I-RYR1 fibers tested. Oscillations abated, and the base line gradually was restored upon removal of halothane by perfusion. Halothane-triggered oscillations were not observed in fibers isolated from either WT-RYR1 or Het T4826I-RYR1 mice.

Compared with WT-RYR1, both Het and Hom T4826I-RYR1 FDB fibers consistently displayed accentuated responses to a 10-s pulse train of electrical stimuli ≤10 Hz. Hom, but not Het, exhibited significantly larger Ca^{2+} transients with pulses delivered at 20 Hz (Fig. 1*B*).

Fig. 2 shows three representative traces from each WT (*A*), Het (*B*), and Hom (*C*) FDB fiber responding to electrical pulse trains and subsequent responses to perfusion of 0.1% halothane. Although perfusion of halothane had negligible influence on $[Ca^{2+}]_{rest}$ in WT, the anesthetic induced a pronounced rise in $[Ca^{2+}]_{rest}$ in Het (92% responded, $n = 39$ fibers tested) and a much larger rise in Hom (100% response, $n = 31$ fibers tested) T4826I-RYR1 FDBs. The massive rise in $[Ca^{2+}]_{rest}$ observed with Hom T4826I-RYR1 fibers exposed to continuous halothane perfusion was invariably transitory and returned toward the base line, whereas the rise in resting Ca^{2+} was

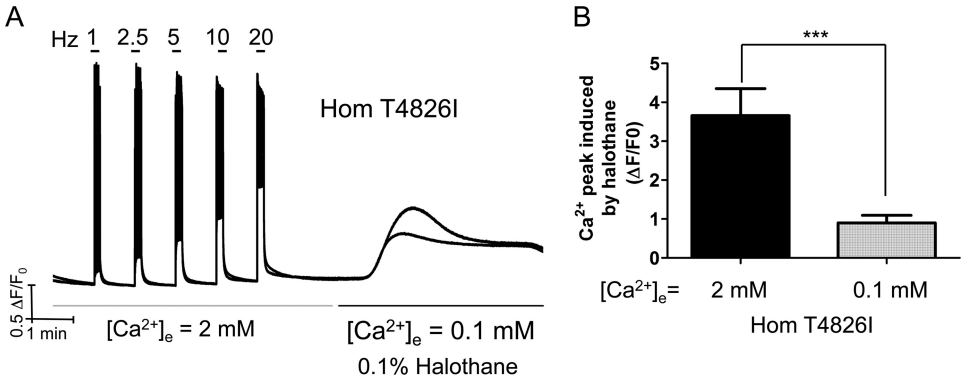

FIGURE 3. **$[Ca^{2+}]_e$ contributes to halothane-triggered peak Ca^{2+} rise in Hom T4826I-RYR1 FDB.** Fibers dissociated from WT-RYR1 and Hom T4826I-RYR1 mice were loaded with Fluo-4 and tested for electrically evoked EC coupling in Ca^{2+}-replete external buffer ($[Ca^{2+}]_e$ = 2 mM). Fibers were then challenged with halothane in the same external buffer whose $[Ca^{2+}]_e$ was reduced with EGTA ($[Ca^{2+}]_e$ = 0.1 mM). *A*, representative traces from two individual Hom T4826I-RYR1 fibers. *B*, comparison of the halothane-triggered peak Ca^{2+} amplitude (mean ± S.E. (*error bars*)) for Hom T4826I-RYR1 fibers with $[Ca^{2+}]_e$ = 2 mM (0.9 ± 0.2; n = 8) and $[Ca^{2+}]_e$ = 0.1 mM (3.7 ± 0.7; n = 4) ($p < 0.001$).

slower and sustained with Het T4826I-RYR1 fibers. In 29% of the Hom T4826I-RYR1 fibers (eight fibers), halothane perfusion initially induced a massive Ca^{2+} rise that was followed by regenerative Ca^{2+} waves having a mean ± S.D. frequency of 3.7 ± 2.1 min^{-1} (Fig. 2*D* and supplemental Movie 1). Neither WT nor Het T4826I-RYR1 FDBs showed oscillatory behavior in response to halothane (not shown). In the absence of halothane, spontaneous Ca^{2+} waves were not observed in 180 Het and 203 Hom T4826I fibers analyzed.

To further evaluate the contribution of Ca^{2+} entry to halothane-triggered Ca^{2+} dysregulation, we first verified the integrity of electrically evoked EC coupling of Hom T4826I-RYR1 FDB fibers in the external solution replete with Ca^{2+} ($[Ca^{2+}]_e$ = 2 mM) and then exchanged the external solution with $[Ca^{2+}]_e$ = 0.1 mM in the presence of 0.1% halothane (Fig. 3*A*). Fig. 3*B* shows that halothane-triggered peak elevation of myoplasmic resting Ca^{2+} is attenuated ~3.5-fold in $[Ca^{2+}]_e$ = 0.1 mM, indicating that significant Ca^{2+} entry contributes to the halothane response in resting Hom T4826I-RYR1 FDB fibers.

Chronically Elevated Cytoplasmic $[Ca^{2+}]_{rest}$ in Adult T4826I-RYR1 Fibers—We previously reported that RYR null 1B5 myotubes transduced with T4826I-RYR1 cDNA results in significantly elevated $[Ca^{2+}]_{rest}$ compared with WT (42). Here we measured $[Ca^{2+}]_{rest}$ in the vastus lateralis of ketamine/xylazine-anesthetized WT, Het, and Hom T4826I-RYR1 mice (results from both sexes combined). Compared with WT muscles, *in vivo* microelectrode measurements showed that myoplasmic $[Ca^{2+}]_{rest}$ was 2.4- and 3.0-fold higher than WT in Het and Hom T4826I-RYR1 muscle fibers (mean ± S.D. $[Ca^{2+}]_{rest}$: 114 ± 3.8, 278 ± 21, and 337 ± 20 nM, respectively, from n = 20–34 fibers/genotype; $p < 0.001$ among the three genotypes). In contrast to $[Ca^{2+}]_{rest}$, the corresponding V_m of these *vastus lateralis* fibers did not differ among the three genotypes (WT = −82 ± 1.3; n = 20 from two mice; Het = −82 ± 1.4; n = 34 from five mice; Hom = −82 ± 1.5; n = 25 from three mice).

Collectively, these data indicate that adult FDB fibers isolated from Het and Hom T4826I-RYR1 mice exhibit heightened sensitivity to halothane, whose magnitude is a function of gene dose, consistent with their relative sensitivities to triggering fulminant MH *in vivo* (1). Moreover, both MH-susceptible genotypes have two basal abnormalities: 1) enhanced gain of EC coupling and 2) chronically elevated $[Ca^{2+}]_{rest}$. We therefore investigated if chronic dysregulation of cellular Ca^{2+} dynamics due to the T4826I-RYR1 mutation in the absence of triggering agents affected mitochondrial bioenergetics and calpain activity, biomarkers known to mediate muscle damage.

Reduced Mitochondrial Respiration and Higher Calpain Activities in Resting T4826I-RYR1 Myotubes—We tested if T4826I-RYR1 mutations influenced OCR and respiratory capacity (RC) in intact muscle cells using a Seahorse XF-24 metabolic flux analyzer. Technical challenges, including inconsistent plating density, precluded making these measurements on FDB fibers; therefore, primary myotubes were used as an alternative. Myotubes from all three genotypes were plated on separate wells of a Seahorse plate at a density of 30,000 cells/well and differentiated into myotubes for 3 days, at which time OCR and RC were measured. In parallel cultures, MitoTracker was used to measure mitochondrial mass. Fig. 4*A* shows a representative OCR experiment performed on the three genotypes. The OCR values are expressed as a percentage of the respective base lines (before the addition of oligomycin). Both Het and Hom T4826I-RYR1 myotubes displayed a significantly lower basal OCR ($p < 0.001$) compared with WT (Fig. 4*B*), and basal OCR was significantly lower with Hom compared with Het T4826I-RYR1 myotubes (p = 0.0167). In order to compare RC across the three genotypes (OCR values after FCCP injection), the results were expressed as area under the curve (corrected for non-mitochondrial rotenone-insensitive OCR). The mean ± S.E. respiratory capacities of Het and Hom T4826I-RYR1 myotubes were significantly lower than that of WT (Fig. 4*C*). Interestingly, the Hom T4826I-RYR1 RC was higher than that of Het ($p < 0.01$).

MitoTracker green, a dye shown to bind mitochondria regardless of membrane potential and a quantitative method for measuring total mitochondrial mass (34, 35), was used to test if the lower RC of the myotubes expressing T4826I-RyR1 was associated with altered mitochondrial content. Fig. 4*D* shows that Het and Hom T4826I-RYR1 myotubes have significantly lower mitochondrial mass than WT myotubes (83.0 ± 1.9 and 67.5 ± 6.6%, respectively).

t-BOC fluorescence was used to determine if chronically elevated myoplasmic $[Ca^{2+}]_{rest}$ levels could promote calpain

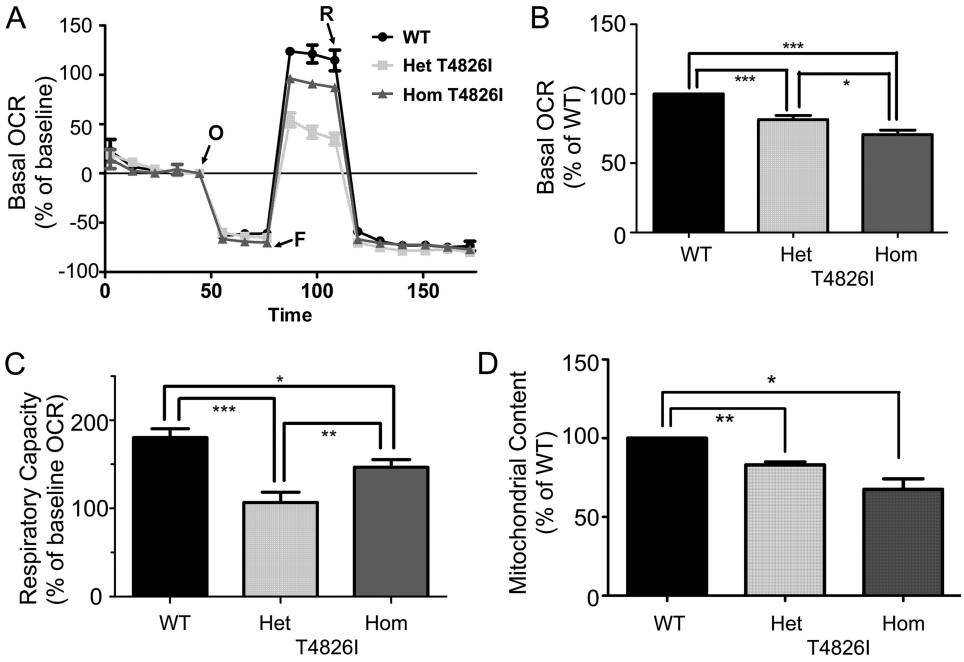

FIGURE 4. **Myotubes isolated from T4826I-RYR1 mice have impaired oxygen consumption and respiratory capacity and lower mitochondrial content.** The basal OCR and RC were evaluated before and after sequential injection of oligomycin, FCCP, and rotenone into the wells of a Seahorse Biosciences flux analyzer. WT, Het, and Hom 4826I-RYR1 myoblasts were plated at 30,000 cells/well and differentiated to myotubes 3 days prior to measuring OCR and RC. A representative experiment is shown in *A*, where OCR was measured simultaneously from the three genotypes before and after sequential injection of mitochondrial inhibitors (oligomycin (*O*), FCCP (*F*), and rotenone (*R*)). Each trace represents the mean ± S.E. (*error bars*) OCR of 5 wells/genotype. The values were normalized to basal OCR (before oligomycin injection). *B*, mean ± S.E. OCR obtained from 25 wells from four independent experiments, indicating that Het and Hom T4826I-RYR1 myotubes have significantly lower basal OCR and RC compared with WT myotubes. The mean ± S.E. basal OCR values were Het = 81.4 ± 3.2 ($p < 0.01$) and Hom = 70.8 ± 3.1% ($p < 0.01$) of WT. *C*, RC measured as OCR after injecting FCCP to uncouple electron transport (after FCCP in *A*). The mean ± S.E. RC values were significantly lower in Het and Hom T4826I-RYR1 compared with WT (59.8 ± 11.3% ($p = 0.034$) and 64.8 ± 8.7% ($p = 0.026$), respectively). *D*, intact myotubes were loaded with 100 nM MitoTracker Green, and the cellular fluorescence was quantitatively measured as described under "Experimental Procedures." The fluorescence values were normalized to protein concentration. Each *bar* represents the mean ± S.E. of $n = 4$ independent experiments, each performed with five replicates. **, $p < 0.01$; *, $p < 0.05$.

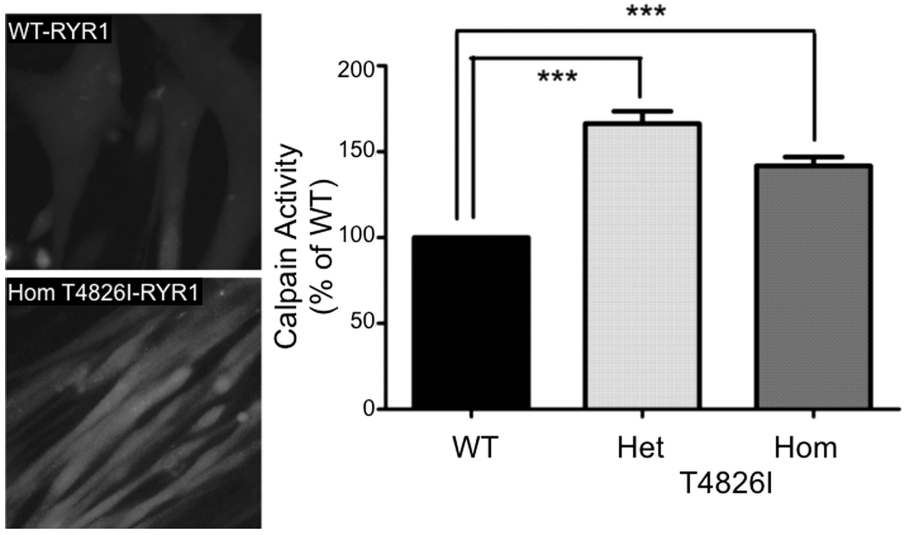

FIGURE 5. **T4826I mutants show enhanced intracellular calpain activity.** *A*, myotube peptidase activity was measured quantitatively using the synthetic substrate *t*-BOC, which is cleaved by intracellular calpain to a fluorescent product using Quantview as described under "Experimental Procedures." *B*, calpain activity summarized, where each *bar* represents the mean ± S.E. (*error bars*) of 100 myotubes/genotype relative to WT (***, $p < 0.001$).

activities associated with muscle damage and degeneration (43). Fig. 5 (*left*) shows representative micrographs, and bar graphs (Fig. 5, *right*) show that both Het and Hom T4826I-RYR1 myotubes have elevated calpain activities that are 170 and 145% of WT (mean *t*-BOC fluorescence of 100 myotubes/genotype normalized to WT).

Expression and Phosphorylation of T4826I-RYR1 Channels Do Not Account for Increased [^{3}H]Ry Binding Capacity—The influence of PKA phosphorylation of RyR1 on channel activity has been debated in the literature (19, 41, 44, 45). Our recent study of R163C-RYR1 isolated from Het mouse muscle indicated higher Ser^{2844} phosphorylation (~31%) compared with

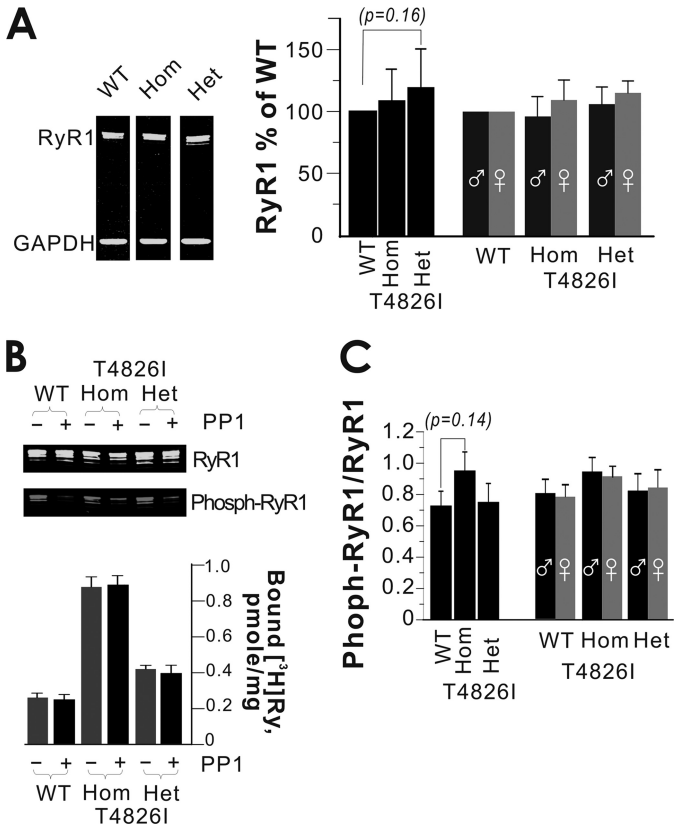

FIGURE 6. **No significant differences in total RYR1 expression or phosphorylation of Ser^{2844}-RYR1 in preparations from WT, Het, or Hom T4826I-RYR1 mice.** *A*, representative Western blot showing the expression of RYR1 probed with monoclonal 34C (total RYR1; green channel). The *bar graph* shows mean ± S.E. (*error bars*) densitometry results for $n = 17$ blots from seven membrane preparations where muscle was pooled from males and females. No differences among the three genotypes for total RYR1 protein expression were detected. In separate preparations, skeletal muscle from males and females were collected, and membranes prepared and blotted separately. *Bar graphs* show mean ± S.E. densitometry results for $n = 6$ blots from two separate membrane preparations. No differences between gender or among genotypes for total RYR1 protein expression were detected. *B*, representative Western blot showing Ser(P)^{2844}-RYR1 levels before and after treatment with PP1. The *bottom panel* summarizes the amount of specific [^{3}H]Ry binding to muscle membranes isolated from WT, Het, and Hom T4826I mice with and without PP1 treatment. PP1 effectively dephosphorylates Ser(P)^{2844}-RYR1 but has no effect on [^{3}H]Ry binding levels, which remain significantly higher in preparations from Het and Hom mutants (also see Fig. 9). *C*, densitometry shows that the relative levels of Ser(P)^{2844}-RYR1/total RYR1 did not significantly differ among the three genotypes (mean ± S.E. for $n = 16$ blots from five membrane preparations) or between genders (mean ± S.E. for $n = 6$ blots from two membrane preparations).

WT-RYR1, although dephosphorylation with protein phosphatase did not restore R163C-RYR1 channel behavior to that observed with WT-RYR1 channels (19). We therefore measured the level of total RYR1 expression and the degree of phosphorylation of Ser^{2844} (Ser(P)^{2844}) in whole membrane fractions from skeletal muscle prepared from WT, Het, and Hom T4826I-RYR1. Fig. 6*A* shows results from a typical Western blot of skeletal muscle membranes probed with monoclonal antibody 34C that recognizes RYR1, indicating that no significant differences were detected in the level of RYR1 protein expression (normalized to GAPDH) among the three genotypes, regardless of whether male and female muscle samples were pooled or separated prior to preparing membranes for Western blotting (Fig. 6*A*, *left*). Blots were probed with both 34C and an antibody that recognizes Ser(P)^{2844}, which showed that unlike in muscles expressing R163C-RYR1, there were no significant differences among the three genotypes in the degree to which RYR1 was phosphorylated (Fig. 6, *B* (*top*) and *C* (*bar plot* of densitometry); $n = 16$ blots from five different preparations).

Het and Hom T4826I-RYR1 preparations display a significantly higher capacity to specifically bind [^{3}H]Ry than WT-RYR1 preparations under defined assay conditions (Fig. 6*B*, *bottom*), which is likely to reflect their inherently higher open probabilities (see below). Although muscle preparations from T4826I-RYR1 mice show similar levels of total RYR1 protein and Ser(P)^{2844} as those from WT, we determined if the level of phosphorylation influences the capacity to bind [^{3}H]Ry to a greater extent in T4826I-RYR1 than WT by exposing membrane preparations to PP1 (see "Experimental Procedures"). Western blotting with and without PP1-treated membranes showed nearly complete dephosphorylation of Ser(P)^{2844} in all three genotypes (Fig. 6*B*, *top*), although the level of [^{3}H]Ry binding remained unchanged regardless of the degree of phosphorylation (Fig. 6*B*, *bottom*).

Het and Hom T4826I-RYR1 Channels Have Inherently Higher Open Probability than WT—WT-RYR1, Het, or Hom T4826-RYR1 channels were incorporated into BLM by induced fusion of SR vesicles. In the presence of 1 μM free cytosolic (*cis*) Ca^{2+}, 2 mM Na_2ATP, and 100 μM free luminal (*trans*) Ca^{2+}, the single channel activity was recorded at a holding potential of −40 mV (applied to *trans*). Fig. 7*A* shows representative current traces from a WT-RYR1 (*top trace*), a Het (*middle trace*), and a Hom (*bottom trace*) channel. Compared with WT-RYR1, the Het T4826I-RYR1 channel exhibited 9-fold higher P_o, with 2.5-fold greater τ_o and ~6-fold shortened τ_o. Hom T4826-RYR1 channels demonstrated even greater deviations compared with WT-RYR1. For example, the Hom T4826-RYR1 shown in Fig. 7*A* displayed ~15-fold higher P_o, ~5-fold greater τ_o, and 10.5-fold shortened τ_o compared with WT-RYR1.

As shown in Fig. 7, *B* and *C*, channels reconstituted from Het T4826I-RYR1 mice produced more heterogeneous gating behavior with a broadly scattered P_o, ranging from 0.19 to 0.71 (mean $P_o = 0.41$; $n = 5$; statistical analysis was not done due to limited data points). This behavior would be expected from random association of WT- and T4826I-RYR1 monomers into functional tetramers as recently described for channels isolated from Het R163C mice (19). Hom T4826-RYR1 channels showed invariantly high P_o behavior (mean $P_o = 0.82$; $n = 10$), which was significantly different from WT-RYR1 (mean $P_o = 0.10$; $n = 12$; $p < 0.0001$).

Analyses of current amplitude distributions from representative channels reconstituted from each genotype are shown in Fig. 8. The most frequent transitions of WT-RYR1 were centered about zero current, the closed channel state (*top*). In marked contrast, the Hom T4826I-RYR1 channel (*bottom*) exhibited most transitions centered about the maximal unitary current amplitude, the full open channel state. Het T4826I-RYR1 channels exhibited an intermediate and broader current amplitude distribution compared with WT-RYR1 and Hom T4826I-RYR1 channels (Fig. 8, *middle*).

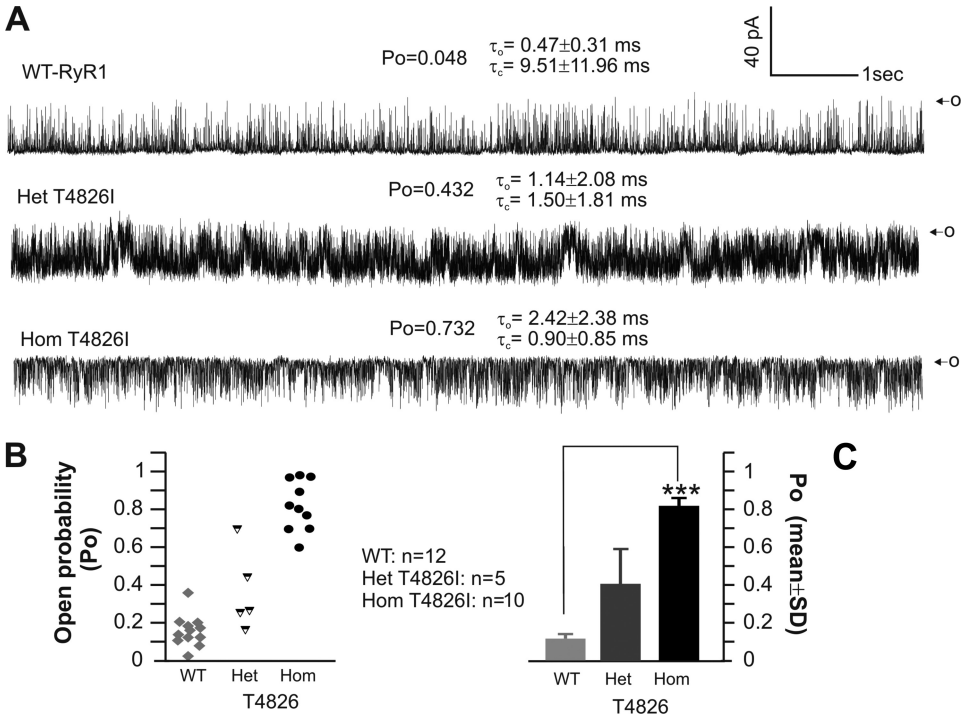

FIGURE 7. **Hom T4826I-RYR1 channels are uniformly hyperactive in BLM.** Single channels were incorporated in BLM in the presence of 1 μM free Ca^{2+}, 2 mM Na_2ATP in *cis* chamber, 100 μM Ca^{2+} in *trans*. *A*, representative 10-s continuous recording for a WT-RYR1 (*top trace*), a Het T4826I-RYR1 (*middle trace*), and Hom T4826I-RYR1 channel currents (*bottom trace*) with their corresponding P_o, τ_o, and τ_c. *O*, maximal single channel current amplitude. *B* and *C*, summary of P_o data for $n = 13$ WT-RYR1, $n = 5$ Het T4826I-RYR1, and $n = 10$ Hom T4826I-RYR1 channels (*B*, scatter plot; *C*, mean ± S.D. (*error bars*)). Channels were reconstituted from three different paired skeletal muscle membrane preparations. ***, $p < 0.0001$.

T4826I-RYR1 Exhibits Altered Sensitivities to Regulation by Ca^{2+} and Mg^{2+}—Ca^{2+} and Mg^{2+} are physiological modulators of RYR1 channel activity (46–48). Using [^{3}H]Ry as a probe to RYR1 channel conformational status, we investigated how the T4826I-RYR1 mutation alters Ca^{2+} regulation of [^{3}H]Ry binding through interactions with high affinity activation sites, and both Ca^{2+} and Mg^{2+} interact with allosterically coupled low affinity sites (49, 50). Fig. 9*A* shows the concentration-effect relationship across a range of Ca^{2+} concentrations from 10^{-8} to 10^{-2} M. The maximum level of [^{3}H]Ry binding at optimal Ca^{2+} was consistently 4- and 9-fold higher for Het and Hom T4826I-RYR1 compared with WT, respectively (Fig. 9*A*, *left*) ($p < 0.01$). Analysis of the Ca^{2+} curves normalized to their respective maxima (Fig. 9*A*, *right*) revealed that both Het and Hom T4826I-RYR1 exhibit higher sensitivity to Ca^{2+} activating at high affinity sites, but only Hom has reduced sensitivity to Ca^{2+} inhibition through low affinity sites (Fig. 9, *A* and *C*). Interestingly, Hom and Het T4826I-RYR1 had reduced sensitivity to Mg^{2+} inhibition through low affinity sites compared with WT (Fig. 9, *B* and *D*) ($p < 0.05$).

Augmented Response of T4826I-RYR1 to Temperature—Fulminant MH can be triggered in Het and Hom T4826I-RYR1 mice in response to halothane and/or heat stress (1). We therefore investigated whether temperature differentially influences the kinetics of [^{3}H]Ry binding to skeletal muscle prepared from the three genotypes. Fig. 10 shows that the observed rate of [^{3}H]Ry binding (k_{obs}) depends significantly on genotype, with the rank order Hom > Het > WT, and temperature (25 *versus* 37 °C) (*A* and *B*). Fig. 10*C* shows that the relative increase in binding rate (normalized to WT) is greater at 37 °C than it is at 25 °C (Fig. 10*C*) and that Hom is more responsive to temperature than Het.

DISCUSSION

As is the case with most RYR1 MHS mutations, heterozygosis for T4825I-RYR1 in humans is sufficient to confer MHS, and individuals homozygous for T4826I-RYR1 have not been described. Although very rare, individuals homozygous for RYR1 mutation C35R (51) and R614C (52) have been described in families with a history of MHS, and muscle biopsies from Hom individuals have increased sensitivity to halothane and caffeine compared with Het individuals (52). Recently, we described that Het and Hom T4826I-RYR1 mice are viable but display distinctly different phenotypic penetrance for triggering fulminant MH with halothane and heat stress. This difference allowed us to uncover a genotype- and sex-dependent susceptibility to pharmacological and environmental stressors that trigger fulminant MH and promote myopathy (1). In this regard, T4826I-RYR1 mice provide unique insights into understanding the genotype-phenotype relationships of MHS mutations *in vivo* and the mechanisms influencing muscle dysfunction and fulminant MH in adult skeletal muscle *in vivo* and *in vitro*.

One important outcome of channel dysfunction in adult muscle fibers expressing T4826I-RYR1 is a chronically elevated myoplasmic $[Ca^{2+}]_{rest}$ under basal (non-triggered) conditions. In this regard, there is a clear gene dose influence on myoplasmic $[Ca^{2+}]_{rest}$ with WT < Het < Hom. Recently Murayama *et al.* (53) did not detect a difference in cytoplasmic $[Ca^{2+}]_{rest}$ in HEK 293 cells transiently transfected with T4826I-RYR1 com-

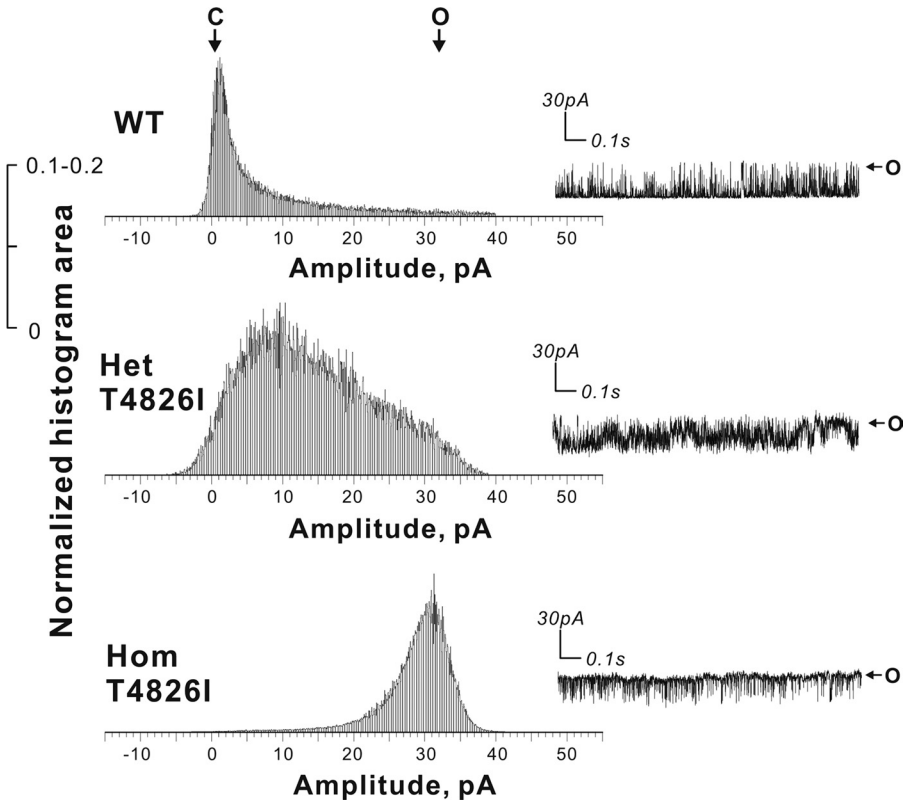

FIGURE 8. **Het and Hom T4826I-RYR1 channels show distinct gating behaviors.** Representative channel current amplitude histograms were obtained for WT-RYR1, Het, and Hom T4826I-RYR1 under identical conditions described in the legend to Fig. 7. WT-RYR1 and T4826I-RYR1 channels show uniform current amplitudes that strongly favor the closed and full open channel states, respectively. Het T4826I-RYR1 channels exhibited broader intermediate states consistent with random association of WT-T4826I RYR1 monomers to form chimeric tetrameric channels. The *insets* show 1.5 s of representative current trace for each genotype.

pared with those expressing WT-RYR1. Several significant methodological differences could account for these divergent results. First, *in vitro* heterologous expression of RyRs in a system where there are no DHPRs to provide negative regulation *versus* measurements made *in vivo* in adult muscle fibers will decrease any difference due to fact that increased numbers of WT-RYR1 protomers will be in the leak conformation (16). This is compounded by the use of Fura 2 ratios with the inherent inaccuracy caused by using an EGTA-based buffer as an indicator *versus* measurements of $[Ca^{2+}]_{rest}$ using calibrated double barreled microelectrodes. Nevertheless, the present results are consistent with those previously reported in adult R163C-RYR1 Het muscle fibers (19) and indicate that chronically elevated $[Ca^{2+}]_{rest}$ may be a common outcome of MHS mutations that promote RYR1 conformations that are leaky (26).

Arguably, the most significant finding in the present study is the uniformly high single channel P_o and high capacity to bind [^{3}H]Ry of Hom T4826I-RYR1 preparations isolated from adult mice when compared with WT. Although the unitary current level and full gating transitions of Hom T4826I-RYR1 channels remain intact, the mutation concomitantly destabilizes the full closed state and stabilizes the full open state of the channel to achieve remarkably high P_o with very tight current distributions, consistent with the formation of a uniform population of T4826I-RYR1 tetramers. Channel gating behavior, rather than differences in RYR1 protein expression or phosphorylation, is responsible for the significantly higher level of [^{3}H]Ry binding observed in Hom muscle preparations when assayed in the presence of optimal Ca^{2+} and is achieved because the inherently stable open channel conformation also stabilizes all [^{3}H]Ry binding sites in their high affinity conformation (54). This interpretation is consistent with the fact that Het T4826I-RYR1 channels display more heterogeneous gating behavior consistent with random assembly of chimeric (WT/T4826I) tetramers and achieve a [^{3}H]Ry occupancy level intermediate between those of WT and Hom. This behavior is similar to those recently described for preparations isolated from Het R163C-RYR1 MHS mice (19). Both Het R163C and T4826I mutations enhance sensitivity to activation by Ca^{2+} (3- and 2-fold compared with WT, respectively), but only the latter mutation confers decreased sensitivity to inhibition by Mg^{2+} in both Het and Hom preparations (~1.5-fold compared with WT) and a decreased sensitivity to Ca^{2+} inactivation in the Hom preparation. Cytoplasmic Mg^{2+} is a physiological negative control of RYR1 channel activity under resting and activating conditions, and impaired regulation by Mg^{2+} has been implicated as an important contributor to MHS (42, 55–57). However, the current results indicate that subtle shifts in regulation by physiological cations cannot fully explain the profound dysfunction of Het and Hom T4826I-RYR1 channels observed here and may involve altered nitrosylation (20) or other covalent modifications.

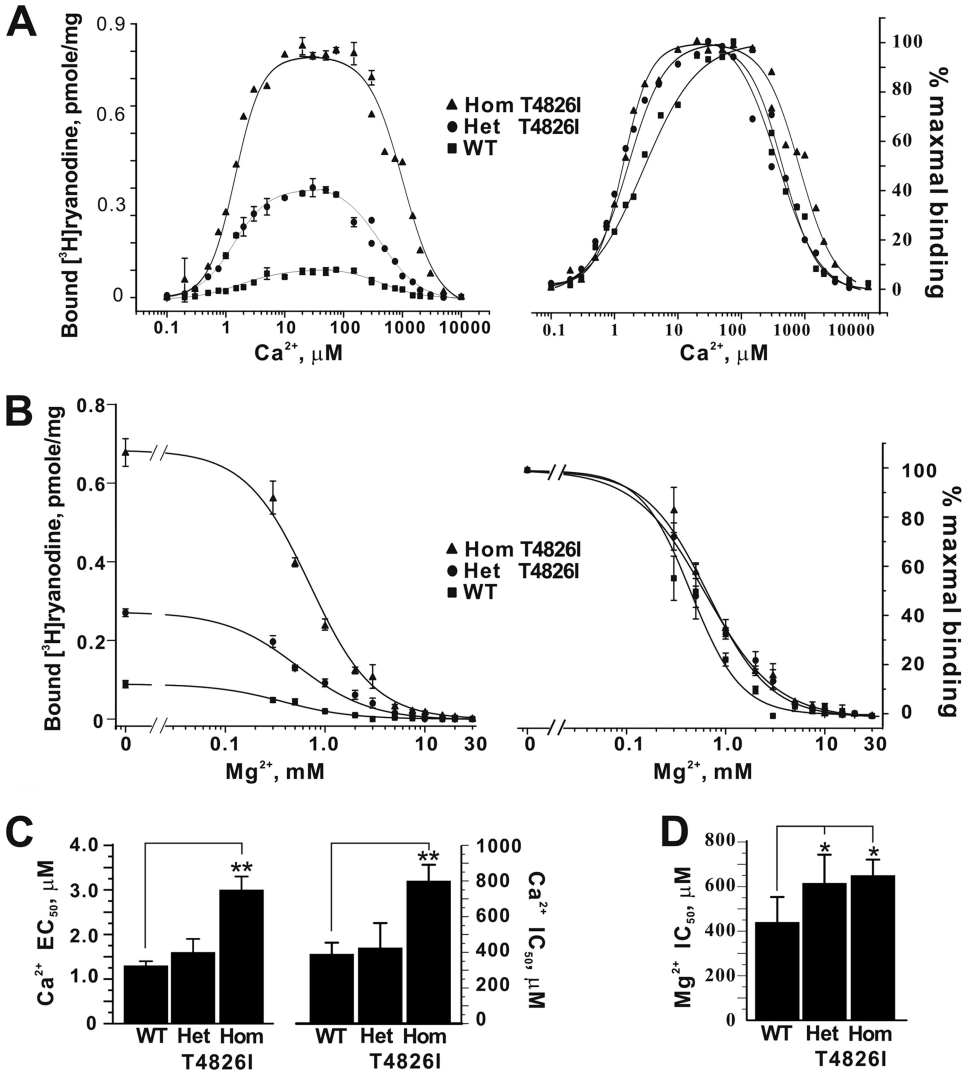

FIGURE 9. **WT, Het, and Hom T4826I-RYR1 differ in their modulation by Ca^{2+} and Mg^{2+}.** Equilibrium [^{3}H]Ry binding (2 nM) was performed at 37 °C for 3 h in the presence of defined [Ca^{2+}] (100 nM to 10 mM) (*A*) or 5 μM Ca^{2+} + Mg^{2+} (0–30 mM) (*B*). EC_{50} and IC_{50} values obtained from curve fit of Ca^{2+} activation/inactivation and Mg^{2+} inhibition are plotted in *C* and *D*, respectively. The data are from 3–4 different skeletal muscle membrane preparations (100 μg/ml) (n = 9–11 (*A* and *C*); n = 8–9 (*B* and *D*)). The significance of difference is denoted as follows: *, $p < 0.05$; **, $p < 0.01$.

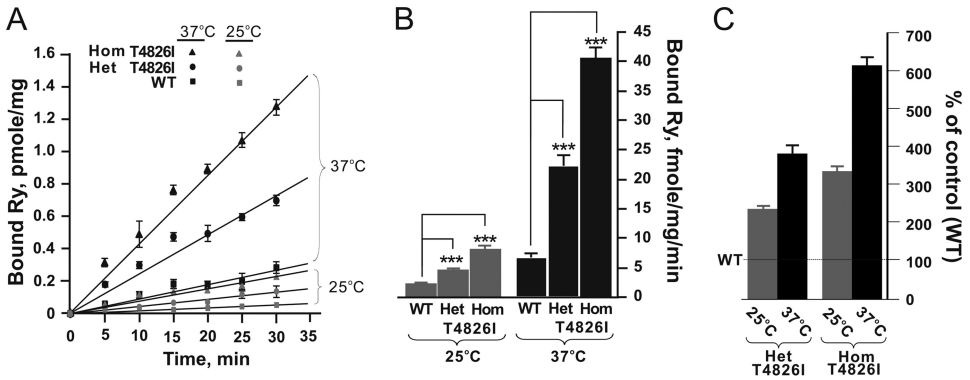

FIGURE 10. **WT, Het, and Hom T4826I-RYR1 differ in sensitivity to temperature.** Initial binding of 5 nM [^{3}H]Ry to 100 μg/ml skeletal muscle membranes were performed at 25 or 37 °C in the presence of 5 μM free Ca^{2+} and determined at 5, 10, 15, 20, 25, and 30 min. *A*, the results are plotted as *rate lines*. *B*, The initial rates were calculated, and k_{obs} values are plotted as *bar graphs*. *C*, the differences in k_{obs} measured with Het and Hom T4826I-RYR1 are plotted relative to k_{obs} WT-RYR1. Statistical analyses indicate significant difference in temperature sensitivity among the three genotypes (***, $p < 0.001$; n = 4 from two different skeletal muscle membrane preparations).

A more significant contributor to channel dysfunction is the location of the mutation within the cytoplasmic loop linking transmembrane segments 4 and 5 (S4-S5). Recently, Murayama *et al.* (53) reported results of substitution scan of the N-terminal half of the putative S4-S5 linker (Thr^{4825}–Ser^{4829}) of RYR1, including T4825I (rabbit sequence). Consistent with our find-

ings with halothane in the current work and our finding of increased sensitivity to caffeine and 4-C*m*C previously (42), HEK 293 cells expressing T4825I-RYR1 exhibited higher sensitivity to caffeine and produced higher P_o channels reconstituted in BLM compared with those expressing WT (53). In this regard, our results from Hom T4826I-RYR1 channels prepared from adult skeletal muscle show even more profound stability of the open state conformation ($P_o > 0.8$ in the presence of suboptimal 1 μM cytoplasmic Ca^{2+}) compared with expressed T4825I-RYR1 ($P_o \sim 0.3$ in the presence of optimal 100 μM cytoplasmic Ca^{2+}) (53).

Although qualitatively similar, several experimental differences could contribute to the quantitative divergence of our single channel results from those of Murayama *et al.* (53), most notable are the BLM solutions having pH of 7.4 *versus* 6.8, 1 μM *versus* 100 μM *cis*-Ca^{2+}, and *trans*-Ca^{2+} of 100 μM *versus* undefined, respectively. Our experimental conditions resulted in a mean P_o for reconstituted WT channels of 0.12 (Fig. 7*C*), which is lower than those reported by Murayama *et al.* (53) for WT channels (mean $P_o \sim 0.19$). Nevertheless, our Hom T4826I-RyR1 channels produced a mean P_o of 0.81 (nearly 8-fold higher than WT), whereas the T4825I-RyR1 channels reconstituted from HEK 293 cells by Murayama *et al.* had a ~1.5-fold higher mean P_o than WT ($P_o \sim 0.19$ for WT and $P_o \sim 0.29$ T4826I-RyR1; Fig. 4*B* in Ref. 53). Interestingly, our BLM results are consistent with both the 7–8-fold higher level of [^{3}H]Ry binding reported in our study (Fig. 9*A*) and the ~7–8-fold increase reported by Murayama *et al.* at 100 μM Ca^{2+} (Fig. 5*B* in Ref. 53).

This distinction is important because it suggests that in addition to the inherent dysregulation imparted by the T4826I mutation, the presence of the mutation over time in the context of its native muscle environment may lead to stable covalent modifications, other than phosphorylation, that contribute to abnormally active channel behavior, and these differences need to be explored in the future.

As for the mechanism by which the T4826I mutation causes RyR1 dysfunction, two possibilities are apparent: 1) impairment of the strong negative feedback regulation provided by protein-protein interactions within the junctional Ca^{2+} release unit, especially the DHPR (16), and 2) increased SR Ca^{2+} leak, possibly mediated by the RyR1 leak conformation (58). Mutation of the α-helical conformation of the S4-S5 linker may be sufficient to impair both of these regulatory mechanism (53). This hypothesis is reasonable given the important role of the S4-S5 linker in gating other ion channels, such as $K_V1.2$ (59, 60). MHS mutations residing within the RYR1 N-terminal region (amino acids 35–609) have been suggested to destabilize domain-domain interactions (61, 62). However, it is clear from the present study that mutations residing within the transmembrane assembly are likely to disrupt channel gating through distinct molecular mechanisms and underscore the allosteric influence of RYR1 mutations that confer MHS.

Ca^{2+} dysregulation triggered by acute halothane exposure of FDB fibers from Het and Hom T4826I-RYR1 male mice is clearly dependent on gene dose. A new finding is that the augmented response to halothane seen in intact Hom FDB fibers involves triggered release from SR Ca^{2+} stores and a significant component of Ca^{2+} entry. Thus, the fulminant MH syndrome is likely to be initiated by disinhibition of RYR1 and exaggerated Ca^{2+} excitation-coupled Ca^{2+} entry and store-operated Ca^{2+} entry as suggested previously (19, 23, 61, 63). A better understanding of how MHS mutations impair coordinated regulation of Ca^{2+} release units may have novel therapeutic implications.

The fact that Hom T4826I-RYR1 mice survive without overt clinical pathology, although consistent with the human condition when homozygosis has been identified (51, 52), raises several fundamentally important issues about the remarkable dysfunction in their Ca^{2+} release channels. In previous studies with Het R163C MHS mice, RYR1 channel dysregulation was associated with significantly reduced Ca^{2+} transient amplitudes evoked by electrical stimuli (*i.e.* EC coupling) in myotubes but not adult FDB fibers (19). The difference in penetrance of the R163C mutation in myotubes and FDB fibers was interpreted as an indication of tighter negative regulation of mutant RYR1 channels within the context of more developed adult junctions present in FDB compared with the peripheral junctions found in myotubes. Here we show that Het and Hom FDB fibers exhibit subtle differences in EC coupling responses although significantly larger than those of WT, and the degree of amplification is gene dose-dependent (Hom > Het). Thus, the location and/or amino acid substitution of an MHS mutation (R163C *versus* T4826I) influences the basal physiological responses of adult fibers. More importantly, the viability of Hom T4826I mice clearly indicates that the inherent dysfunction of RYR1 channels must be under extremely strong negative regulation by the DHPR in the context of adult muscle fibers because preferential targeting of WT channels to the junctions is not possible. However, another consequence of the mutation is to increase the vulnerability of disengaging negative regulation of the RYR1 channel when exposed to triggering agents.

MHS mutations do produce adaptations that lead to chronic elevations in cytoplasmic $[Ca^{2+}]_{rest}$ and reactive oxygen species that are associated with bioenergetic adaptations in muscle mitochondria (20, 28). Such adaptations may promote muscle damage whose rate of onset, morphological manifestations, and severity depend on the location of the mutation, zygosity, and other factors, such as sex (1). Understanding the mechanisms that limit and promote fulminant MH and the potential damage of highly dysfunctional MHS RYR1 channels is central to understanding the etiology of this disorder.

Acknowledgments—We thank Isela T. Padilla and Benjamin Yuen for excellent technical support for [^{3}H]Ry binding, Western blotting, and BLM experiments.

REFERENCES

1. Yuen, B. T., Boncompagni, S., Feng, W., Yang, T., Lopez, J. R., Matthaei, K. I., Goth, S. R., Protasi, F., Franzini-Armstrong, C., Allen, P. D., and Pessah, I. N. (2011) Mice expressing T4826I-RYR1 are viable but exhibit sex- and genotype-dependent susceptibility to malignant hyperthermia and muscle damage. *FASEB J.* doi:22131268
2. Zhou, J., Allen, P. D., Pessah, I. N., and Naguib, M. (2010) Neuromuscular Disorders and Malignant Hyperthermia. in *Miller's Anesthesia* (Miller, R. D., ed) pp. 1171–1196, 7th Ed., Churchill Livingstone, Philadelphia, PA
3. Litman, R. S., and Rosenberg, H. (2005) Malignant hyperthermia. Update on susceptibility testing. *JAMA* **293,** 2918–2924
4. Robinson, R., Carpenter, D., Shaw, M. A., Halsall, J., and Hopkins, P. (2006)

Mutations in RYR1 in malignant hyperthermia and central core disease. *Hum. Mutat.* **27,** 977–989
5. Brady, J. E., Sun, L. S., Rosenberg, H., and Li, G. (2009) Prevalence of malignant hyperthermia due to anesthesia in New York State, 2001–2005. *Anesth. Analg.* **109,** 1162–1166
6. Robinson, R. L., Anetseder, M. J., Brancadoro, V., van Broekhoven, C., Carsana, A., Censier, K., Fortunato, G., Girard, T., Heytens, L., Hopkins, P. M., Jurkat-Rott, K., Klinger, W., Kozak-Ribbens, G., Krivosic, R., Monnier, N., Nivoche, Y., Olthoff, D., Rueffert, H., Sorrentino, V., Tegazzin, V., and Mueller, C. R. (2003) Recent advances in the diagnosis of malignant hyperthermia susceptibility. How confident can we be of genetic testing? *Eur. J. Hum. Genet.* **11,** 342–348
7. Carpenter, D., Morris, A., Robinson, R. L., Booms, P., Iles, D., Halsall, P. J., Steele, D., Hopkins, P. M., and Shaw, M. A. (2009) Analysis of RYR1 haplotype profile in patients with malignant hyperthermia. *Ann. Hum. Genet.* **73,** 10–18
8. McCarthy, T. V., Quane, K. A., and Lynch, P. J. (2000) Ryanodine receptor mutations in malignant hyperthermia and central core disease. *Hum. Mutat.* **15,** 410–417
9. Louis, C. F., Balog, E. M., and Fruen, B. R. (2001) Malignant hyperthermia. An inherited disorder of skeletal muscle Ca^{+} regulation. *Biosci. Rep.* **21,** 155–168
10. Jurkat-Rott, K., Lerche, H., and Lehmann-Horn, F. (2002) Skeletal muscle channelopathies. *J. Neurol.* **249,** 1493–1502
11. Stewart, S. L., Hogan, K., Rosenberg, H., and Fletcher, J. E. (2001) Identification of the Arg1086His mutation in the α subunit of the voltage-dependent calcium channel (CACNA1S) in a North American family with malignant hyperthermia. *Clin. Genet.* **59,** 178–184
12. Monnier, N., Krivosic-Horber, R., Payen, J. F., Kozak-Ribbens, G., Nivoche, Y., Adnet, P., Reyford, H., and Lunardi, J. (2002) Presence of two different genetic traits in malignant hyperthermia families. Implication for genetic analysis, diagnosis, and incidence of malignant hyperthermia susceptibility. *Anesthesiology* **97,** 1067–1074
13. Toppin, P. J., Chandy, T. T., Ghanekar, A., Kraeva, N., Beattie, W. S., and Riazi, S. (2010) A report of fulminant malignant hyperthermia in a patient with a novel mutation of the CACNA1S gene. *Can. J. Anaesth.* **57,** 689–693
14. Carpenter, D., Ismail, A., Robinson, R. L., Ringrose, C., Booms, P., Iles, D. E., Halsall, P. J., Steele, D., Shaw, M. A., and Hopkins, P. M. (2009) A RYR1 mutation associated with recessive congenital myopathy and dominant malignant hyperthermia in Asian families. *Muscle Nerve* **40,** 633–639
15. Nakai, J., Dirksen, R. T., Nguyen, H. T., Pessah, I. N., Beam, K. G., and Allen, P. D. (1996) Enhanced dihydropyridine receptor channel activity in the presence of ryanodine receptor. *Nature* **380,** 72–75
16. Eltit, J. M., Li, H., Ward, C. W., Molinski, T., Pessah, I. N., Allen, P. D., and Lopez, J. R. (2011) Orthograde dihydropyridine receptor signal regulates ryanodine receptor passive leak. *Proc. Natl. Acad. Sci. U.S.A.* **108,** 7046–7051
17. Yang, T., Riehl, J., Esteve, E., Matthaei, K. I., Goth, S., Allen, P. D., Pessah, I. N., and Lopez, J. R. (2006) Pharmacologic and functional characterization of malignant hyperthermia in the R163C RyR1 knock-in mouse. *Anesthesiology* **105,** 1164–1175
18. Chelu, M. G., Goonasekera, S. A., Durham, W. J., Tang, W., Lueck, J. D., Riehl, J., Pessah, I. N., Zhang, P., Bhattacharjee, M. B., Dirksen, R. T., and Hamilton, S. L. (2006) Heat- and anesthesia-induced malignant hyperthermia in an RyR1 knock-in mouse. *FASEB J.* **20,** 329–330
19. Feng, W., Barrientos, G. C., Cherednichenko, G., Yang, T., Padilla, I. T., Truong, K., Allen, P. D., Lopez, J. R., and Pessah, I. N. (2011) Functional and biochemical properties of ryanodine receptor type 1 channels from heterozygous R163C malignant hyperthermia-susceptible mice. *Mol. Pharmacol.* **79,** 420–431
20. Durham, W. J., Aracena-Parks, P., Long, C., Rossi, A. E., Goonasekera, S. A., Boncompagni, S., Galvan, D. L., Gilman, C. P., Baker, M. R., Shirokova, N., Protasi, F., Dirksen, R., and Hamilton, S. L. (2008) RyR1 *S*-nitrosylation underlies environmental heat stroke and sudden death in Y522S RyR1 knockin mice. *Cell* **133,** 53–65
21. Boncompagni, S., Rossi, A. E., Micaroni, M., Hamilton, S. L., Dirksen, R. T., Franzini-Armstrong, C., and Protasi, F. (2009) Characterization and temporal development of cores in a mouse model of malignant hyperthermia. *Proc. Natl. Acad. Sci. U.S.A.* **106,** 21996–22001
22. Maclennan, D. H., and Zvaritch, E. (2011) Mechanistic models for muscle diseases and disorders originating in the sarcoplasmic reticulum. *Biochim. Biophys. Acta* **1813,** 948–964
23. Cherednichenko, G., Ward, C. W., Feng, W., Cabrales, E., Michaelson, L., Samso, M., López, J. R., Allen, P. D., and Pessah, I. N. (2008) Enhanced excitation-coupled calcium entry in myotubes expressing malignant hyperthermia mutation R163C is attenuated by dantrolene. *Mol. Pharmacol.* **73,** 1203–1212
24. Andronache, Z., Hamilton, S. L., Dirksen, R. T., and Melzer, W. (2009) A retrograde signal from RyR1 alters DHP receptor inactivation and limits window Ca^{2+} release in muscle fibers of Y522S RyR1 knock-in mice. *Proc. Natl. Acad. Sci. U.S.A.* **106,** 4531–4536
25. Bannister, R. A., Estève, E., Eltit, J. M., Pessah, I. N., Allen, P. D., López, J. R., and Beam, K. G. (2010) A malignant hyperthermia-inducing mutation in RYR1 (R163C). Consequent alterations in the functional properties of DHPR channels. *J. Gen. Physiol.* **135,** 629–640
26. Yang, T., Esteve, E., Pessah, I. N., Molinski, T. F., Allen, P. D., and López, J. R. (2007) Elevated resting $[Ca^{2+}]_i$ in myotubes expressing malignant hyperthermia RyR1 cDNAs is partially restored by modulation of passive calcium leak from the SR. *Am. J. Physiol. Cell Physiol.* **292,** C1591–C1598
27. López, J. R., Alamo, L. A., Jones, D., Papp, L., Allen, P., Gergely, J., and Streter, F. (1985) Determination of intracellular free calcium concentration, *in vivo*, in swine susceptible to malignant hyperthermia syndrome. *Acta Cient. Venez.* **36,** 102–104
28. Giulivi, C., Ross-Inta, C., Omanska-Klusek, A., Napoli, E., Sakaguchi, D., Barrientos, G., Allen, P. D., and Pessah, I. N. (2011) Basal bioenergetic abnormalities in skeletal muscle from ryanodine receptor malignant hyperthermia-susceptible R163C knock-in mice. *J. Biol. Chem.* **286,** 99–113
29. Brown, R. L., Pollock, A. N., Couchman, K. G., Hodges, M., Hutchinson, D. O., Waaka, R., Lynch, P., McCarthy, T. V., and Stowell, K. M. (2000) A novel ryanodine receptor mutation and genotype-phenotype correlation in a large malignant hyperthermia New Zealand Maori pedigree. *Hum. Mol. Genet.* **9,** 1515–1524
30. Cherednichenko, G., Hurne, A. M., Fessenden, J. D., Lee, E. H., Allen, P. D., Beam, K. G., and Pessah, I. N. (2004) Conformational activation of Ca^{2+} entry by depolarization of skeletal myotubes. *Proc. Natl. Acad. Sci. U.S.A.* **101,** 15793–15798
31. Hurne, A. M., O'Brien, J. J., Wingrove, D., Cherednichenko, G., Allen, P. D., Beam, K. G., and Pessah, I. N. (2005) Ryanodine receptor type 1 (RyR1) mutations C4958S and C4961S reveal excitation-coupled calcium entry (ECCE) is independent of sarcoplasmic reticulum store depletion. *J. Biol. Chem.* **280,** 36994–37004
32. Rando, T. A., and Blau, H. M. (1997) Methods for myoblast transplantation. *Methods Cell Biol.* **52,** 261–272
33. Barrientos, G., Bose, D. D., Feng, W., Padilla, I., and Pessah, I. N. (2009) The Na^{+}/Ca^{2+} exchange inhibitor 2-(2-(4-(4-nitrobenzyloxy)phenyl)ethyl)isothiourea methanesulfonate (KB-R7943) also blocks ryanodine receptors type 1 (RyR1) and type 2 (RyR2) channels. *Mol. Pharmacol.* **76,** 560–568
34. Civitarese, A. E., Ukropcova, B., Carling, S., Hulver, M., DeFronzo, R. A., Mandarino, L., Ravussin, E., and Smith, S. R. (2006) Role of adiponectin in human skeletal muscle bioenergetics. *Cell Metab.* **4,** 75–87
35. Pendergrass, W., Wolf, N., and Poot, M. (2004) Efficacy of MitoTracker Green and CMXrosamine to measure changes in mitochondrial membrane potentials in living cells and tissues. *Cytometry A* **61,** 162–169
36. Gailly, P., De Backer, F., Van Schoor, M., and Gillis, J. M. (2007) *In situ* measurements of calpain activity in isolated muscle fibres from normal and dystrophin-lacking mdx mice. *J. Physiol.* **582,** 1261–1275
37. Saito, A., Seiler, S., Chu, A., and Fleischer, S. (1984) Preparation and morphology of sarcoplasmic reticulum terminal cisternae from rabbit skeletal muscle. *J. Cell Biol.* **99,** 875–885
38. Mack, W. M., Zimányi, I., and Pessah, I. N. (1992) Discrimination of multiple binding sites for antagonists of the calcium release channel complex of skeletal and cardiac sarcoplasmic reticulum. *J. Pharmacol. Exp. Ther.* **262,** 1028–1037

39. Brooks, S. P., and Storey, K. B. (1992) Bound and determined. A computer program for making buffers of defined ion concentrations. *Anal. Biochem.* **201,** 119–126
40. Airey, J. A., Beck, C. F., Murakami, K., Tanksley, S. J., Deerinck, T. J., Ellisman, M. H., and Sutko, J. L. (1990) Identification and localization of two triad junctional foot protein isoforms in mature avian fast twitch skeletal muscle. *J. Biol. Chem.* **265,** 14187–14194
41. Reiken, S., Lacampagne, A., Zhou, H., Kherani, A., Lehnart, S. E., Ward, C., Huang, F., Gaburjakova, M., Gaburjakova, J., Rosemblit, N., Warren, M. S., He, K. L., Yi, G. H., Wang, J., Burkhoff, D., Vassort, G., and Marks, A. R. (2003) PKA phosphorylation activates the calcium release channel (ryanodine receptor) in skeletal muscle: defective regulation in heart failure. *J. Cell Biol.* **160,** 919–928
42. Yang, T., Ta, T. A., Pessah, I. N., and Allen, P. D. (2003) Functional defects in six ryanodine receptor isoform-1 (RyR1) mutations associated with malignant hyperthermia and their impact on skeletal excitation-contraction coupling. *J. Biol. Chem.* **278,** 25722–25730
43. Vinciguerra, M., Musaro, A., and Rosenthal, N. (2010) Regulation of muscle atrophy in aging and disease. *Adv. Exp. Med. Biol.* **694,** 211–233
44. Hain, J., Nath, S., Mayrleitner, M., Fleischer, S., and Schindler, H. (1994) Phosphorylation modulates the function of the calcium release channel of sarcoplasmic reticulum from skeletal muscle. *Biophys. J.* **67,** 1823–1833
45. Sonnleitner, A., Fleischer, S., and Schindler, H. (1997) Gating of the skeletal calcium release channel by ATP is inhibited by protein phosphatase 1 but not by Mg^{2+}. *Cell Calcium* **21,** 283–290
46. Pessah, I. N., Stambuk, R. A., and Casida, J. E. (1987) Ca^{2+}-activated ryanodine binding. Mechanisms of sensitivity and intensity modulation by Mg^{2+}, caffeine, and adenine nucleotides. *Mol. Pharmacol.* **31,** 232–238
47. Pessah, I. N., Waterhouse, A. L., and Casida, J. E. (1985) The calcium-ryanodine receptor complex of skeletal and cardiac muscle. *Biochem. Biophys. Res. Commun.* **128,** 449–456
48. Meissner, G. (2002) Regulation of mammalian ryanodine receptors. *Front. Biosci.* **7,** d2072–d2080
49. Voss, A. A., Allen, P. D., Pessah, I. N., and Perez, C. F. (2008) Allosterically coupled calcium and magnesium binding sites are unmasked by ryanodine receptor chimeras. *Biochem. Biophys. Res. Commun.* **366,** 988–993
50. Laver, D. R., Baynes, T. M., and Dulhunty, A. F. (1997) Magnesium inhibition of ryanodine-receptor calcium channels. Evidence for two independent mechanisms. *J. Membr. Biol.* **156,** 213–229
51. Lynch, P. J., Krivosic-Horber, R., Reyford, H., Monnier, N., Quane, K., Adnet, P., Haudecoeur, G., Krivosic, I., McCarthy, T., and Lunardi, J. (1997) Identification of heterozygous and homozygous individuals with the novel RYR1 mutation Cys35Arg in a large kindred. *Anesthesiology* **86,** 620–626
52. Rueffert, H., Olthoff, D., Deutrich, C., Thamm, B., and Froster, U. G. (2001) Homozygous and heterozygous Arg614Cys mutations (1840C→T) in the ryanodine receptor gene co-segregate with malignant hyperthermia susceptibility in a German family. *Br. J. Anaesth.* **87,** 240–245
53. Murayama, T., Kurebayashi, N., Oba, T., Oyamada, H., Oguchi, K., Sakurai, T., and Ogawa, Y. (2011) Role of amino-terminal half of the S4-S5 linker in type 1 ryanodine receptor (RyR1) channel gating. *J. Biol. Chem.* **286,** 35571–35577
54. Pessah, I. N., and Zimanyi, I. (1991) Characterization of multiple [^{3}H]ryanodine binding sites on the Ca^{2+} release channel of sarcoplasmic reticulum from skeletal and cardiac muscle. Evidence for a sequential mechanism in ryanodine action. *Mol. Pharmacol.* **39,** 679–689
55. Owen, V. J., Taske, N. L., and Lamb, G. D. (1997) Reduced Mg^{2+} inhibition of Ca^{2+} release in muscle fibers of pigs susceptible to malignant hyperthermia. *Am. J. Physiol.* **272,** C203–C211
56. Laver, D. R., Owen, V. J., Junankar, P. R., Taske, N. L., Dulhunty, A. F., and Lamb, G. D. (1997) Reduced inhibitory effect of Mg^{2+} on ryanodine receptor-Ca^{2+} release channels in malignant hyperthermia. *Biophys. J.* **73,** 1913–1924
57. Lamb, G. D. (1993) Ca^{2+} inactivation, Mg^{2+} inhibition, and malignant hyperthermia. *J. Muscle Res. Cell Motil.* **14,** 554–556
58. Pessah, I. N., Molinski, T. F., Meloy, T. D., Wong, P., Buck, E. D., Allen, P. D., Mohr, F. C., and Mack, M. M. (1997) Bastadins relate ryanodine-sensitive and -insensitive Ca^{2+} efflux pathways in skeletal SR and BC3H1 cells. *Am. J. Physiol.* **272,** C601–C614
59. Long, S. B., Campbell, E. B., and Mackinnon, R. (2005) Crystal structure of a mammalian voltage-dependent Shaker family K^+ channel. *Science* **309,** 897–903
60. Long, S. B., Campbell, E. B., and Mackinnon, R. (2005) Voltage sensor of Kv1.2. Structural basis of electromechanical coupling. *Science* **309,** 903–908
61. Kobayashi, S., Bannister, M. L., Gangopadhyay, J. P., Hamada, T., Parness, J., and Ikemoto, N. (2005) Dantrolene stabilizes domain interactions within the ryanodine receptor. *J. Biol. Chem.* **280,** 6580–6587
62. Murayama, T., Oba, T., Hara, H., Wakebe, K., Ikemoto, N., and Ogawa, Y. (2007) Postulated role of interdomain interaction between regions 1 and 2 within type 1 ryanodine receptor in the pathogenesis of porcine malignant hyperthermia. *Biochem. J.* **402,** 349–357
63. Zhao, X., Weisleder, N., Han, X., Pan, Z., Parness, J., Brotto, M., and Ma, J. (2006) Azumolene inhibits a component of store-operated calcium entry coupled to the skeletal muscle ryanodine receptor. *J. Biol. Chem.* **281,** 33477–33486